

Rate-Fidelity Tradeoffs in All-Photonic and Memory-Equipped Quantum Switches

Panagiotis Promponas, Leonardo Bacciottini, Paul Polakos, Gayane Vardoyan, Don Towsley, and Leandros Tassioulas

Abstract—Quantum entanglement switches are a key building block for early quantum networks, and a central design question is whether near-term devices should use only optical components and photonic qubits or also incorporate quantum memories. We compare two architectures: an all-photonic entanglement generation switch (EGS) that repeatedly attempts Bell-state measurements (BSMs) without storing qubits, and a quantum memory-equipped switch that buffers entanglement and triggers measurements only when heralded connectivity is available (*herald-then-swap* control). These two designs trade off simple, memoryless operation that avoids decoherence and memory-induced latency against heralding-based control that buffers entanglement to use BSMs more efficiently. We formalize both models under a common hardware abstraction and characterize their achievable rate-fidelity regions, yielding a benchmarking methodology that translates hardware and protocol parameters into network-level performance. Numerical evaluation quantifies the rate-fidelity tradeoffs of both models, identifies operating regions in which each architecture dominates, and shows how hardware and protocol knobs can be tuned to meet application-specific targets.

I. INTRODUCTION

Quantum networks that distribute high-fidelity entanglement between distant users underpin applications in secure communication, distributed sensing, and distributed quantum computing [1], [2]. A central challenge is that in lossy optical channels, attenuation causes the success probability of each entanglement-generation attempt to decrease exponentially with distance. This limitation introduces the need for intermediary network nodes, such as quantum repeaters [3] and switches [4], that employ entanglement swapping to establish entanglement between non-adjacent clients.

The evolution from quantum repeaters to multi-user quantum switches introduces a new layer of network-level complexity: the switch must allocate shared resources and schedule entanglement swapping under contention among many user pairs, on top of the underlying physical-layer error processes. The quantum switch is a network node connected to three or more other nodes. It functions as a two-sided queuing system [5]: on one side, requests for end-to-end entanglement arrive, while on the other, probabilistic link-level entanglement

generation (LLEG) produces Bell pairs [6] that must be consumed through entanglement swaps to serve requests.

A large body of work considers a variety of quantum switching models [4], [7]. A useful taxonomy based on the principal architectural tradeoff between hardware simplicity and control intelligence is rooted in the use of quantum memories and the resulting operational logic. This categorization provides a framework for grasping the landscape of current research and motivates the selection of the models analyzed in this paper.

The first major class of switch architectures comprises all-photonic hardware [8] that performs entanglement swapping directly on arriving photons, without storing qubits in quantum memories at the switch. In these architectures, often termed entanglement generation switches (EGS) [7], [9], [10], the switch, in the absence of quantum memories, cannot herald successful link-level entanglement (LLE) attempts prior to performing a Bell-state measurement (BSM). Moreover, BSMs are carried out by a set of Bell-state analyzers (BSAs), each of which can be assigned to any user pair. The lack of heralding forces the switch to trigger BSMs “blindly” on preassigned pairs. Hence, a BSA is often triggered when at most one of the two clients has a successful LLE (i.e., an entangled photon reaches the corresponding BSA), so no end-to-end entangled pair is produced. Recent work explores resource allocation schemes for EGSes, including on-demand blocking models that drop requests when resources are unavailable [9], and load-balancing policies that poll nodes for requests [10].

The second class of architectures incorporates quantum memories to enable more sophisticated, dynamic control logic. The operational paradigm of these switches is “herald-then-swap”. In this model, LLEG is first attempted between each client and the switch. The success of each attempt is signaled to the switch’s controller via a “herald” message. The switch makes a scheduling decision after this connectivity-acquisition phase. The controller, now aware of the set of available Bell pairs, can perform an optimal matching, pairing occupied memories to entanglement swapping operations. This approach enables more efficient use of the stored Bell pairs, since BSM attempts are applied only to heralded links. The memory-enabled switch has been the subject of extensive analysis characterizing its throughput region, developing scheduling policies [11], [12], [13], [14], and analyzing the impact of memory decoherence [15], [16], [5].

These two architectures raise a concrete design question: for a given hardware stack and target application, should one deploy an all-photonic or a memory-equipped switch? Quantum memories can, in principle, boost end-to-end rates and

This work was supported by the Army Research Office MURI under the project number W911NF2110325, by the QuantumCT project, and by the National Science Foundation under project number CNS 2402862.

P. Promponas (panagiotis.promponas@yale.edu) and L. Tassioulas are with the Department of Electrical and Computer Engineering, Yale University, New Haven, CT, USA.

L. Bacciottini, G. Vardoyan and D. Towsley are with the University of Massachusetts, Amherst, MA, USA.

P. Polakos is with Einblick LLC, Marlboro, NJ, USA.

Fidelities, but if coherence times are short or heralding delays are large, a memory-based design can lose this advantage and even underperform compared to a simpler all-photon switch. Thus, architectural superiority is regime-dependent rather than absolute. This paper makes that choice explicit by placing both models in a common abstraction and quantifying their achievable rate–fidelity tradeoffs under realistic hardware assumptions. Our key contributions are:

- We define mathematically precise models for both all-photon and quantum memory-equipped switches, specifying their control strategies, physical resource assumptions, and operational logic.
- We derive closed-form characterizations of the achievable throughput and fidelity under each model, explicitly quantifying how hardware parameters impact end-to-end entanglement performance. Building on this, we develop a benchmarking methodology that provides a unified basis for comparing the two architectures, links low-level hardware parameters to network-level performance, and identifies operational regimes in which each architecture is superior.
- Numerical evaluation quantifies the rate-fidelity trade-offs of both models, and shows how hardware and protocol knobs can be tuned to meet application-specific targets.

II. PRELIMINARIES

A. System Description

We consider a star-topology quantum network with a central switch node connected to N client nodes. Let \mathcal{N} be the node set and $\mathcal{F} \triangleq \{(i, j) : i < j, i, j \in \mathcal{N}\}$. We will use \mathcal{F} to avoid double-counting node pairs and refer to each $(i, j) \in \mathcal{F}$ as an end-to-end flow. The total number of flows is thus $F \triangleq \binom{N}{2} = |\mathcal{F}|$. The switch generates and distributes entangled qubit pairs (Bell pairs) between the clients. Each node is equipped with quantum memories to store qubits until end-to-end entanglement is established. The switch can perform at most B BSMs in parallel to generate end-to-end Bell pairs due to hardware limitations (e.g., it has B BSAs). We assume time-slotted operation. The detailed timing of LLEG attempts, BSMs, and heralding is model-dependent and is specified separately for the EGS and memory-equipped switch models.

B. Fidelity and Quantum Noise Model

Entanglement fidelity quantifies how close a generated state is to a target Bell state, and different applications impose different fidelity requirements. We model noisy entangled states as Werner states, a one-parameter family of mixed states that captures imperfections via the Werner parameter $w \in [0, 1]$. A Werner state for a pair of qubits is expressed as:

$$\rho_w = w |\Phi^+\rangle \langle \Phi^+| + (1-w) \frac{\mathbb{I}}{4},$$

where $|\Phi^+\rangle = \frac{1}{\sqrt{2}}(|00\rangle + |11\rangle)$ is one of the reference Bell states, $\mathbb{I}/4$ is the completely mixed state, and $w \in [0, 1]$ is the Werner parameter. The fidelity of such a state is $F_w = \frac{3w+1}{4}$. When two Werner states with Werner parameters w_1 and

w_2 are swapped with perfect operations, the resulting state’s Werner parameter is simply the product $w_1 \cdot w_2$. Even if the actual entangled state is not a Werner state, such an approximation provides lower bounds for fidelity analysis under an appropriate set of assumptions [17].

A depolarizing channel with parameter $q \in [0, 1]$ acting on a Werner state simply replaces its Werner parameter w with $w \cdot q$. We model the fidelity degradation of the swapped pair using a depolarizing channel with parameter q_{BSM} . Independently, the probability that a BSM attempt succeeds is captured by p_{BSA} (for BSAs in the EGS model) or p_{swap} (for the memory-assisted model); these parameters affect the end-to-end generation rates rather than the output-state fidelity. We also model quantum decoherence in the memories as a depolarizing channel with parameter $e^{-\tau/T}$, where T is the quantum memory coherence time (assumed equal for all memories), and τ is the time spent in memory.

C. Link-level Entanglement Generation Model

We denote by link-level entanglement generation (LLEG) the protocol that generates and distributes Bell pairs between a client and the switch; the resulting Bell pair is referred to as LLE. While details depend on the hardware platform, most implementations share a common structure: they use sources (e.g., Spontaneous Parametric Down-Conversion (SPDC) [18] or emitters [19] based on quantum dots, color centers, or trapped ions) that send entangled photons along the client–switch link. LLEG is inherently probabilistic and requires heralding. To differentiate between this heralding and the one needed to establish an end-to-end entanglement between distant nodes, we call this link-level heralding. A hardware-independent abstraction can be described by a common set of parameters. For LLEG between i and the switch, define:

Success probability p_i : Probability that an LLEG attempt successfully produces a Bell pair between i and the switch.

Heralding overhead τ_{hrl} : The *overhead* time needed *after* a successful LLE has been established (e.g., one memory in a node and the switch share an entangled pair) to herald the link-level entanglement in the switch (so it can learn connectivity). Node-side confirmation for the LLE can occur in parallel and does not affect switch operation, since nodes ultimately learn success/failure via the end-to-end entanglement heralding.

Werner parameter w_i : The Werner parameter associated with a successful LLE of node i . Hence, w_i also accounts for decoherence on the qubits involved in this LLE while the switch awaits for the link-level heralding signals.

Tuning parameter β : A controllable property of the source (e.g., pump power for SPDC or brightness for emitters [17]) that affects p_i and w_i . Increasing β raises p_i but lowers w_i due to multi-pair emissions. Thus, p_i and w_i are functions of β , denoted as $p_i(\beta)$ and $w_i(\beta)$.

Attempt period Δt : Minimum time separation between the start of two consecutive LLEG attempts on a given link. For example, with an SPDC source that makes a single pair-generation attempt per optical pulse, $\Delta t = 1/f_{\text{pulse}}$, where f_{pulse} is the source pulse repetition rate (Hz).

Multiplexing degree S_i : Number of parallel LLEG attempts that can be performed between client i and the switch. It captures spatial or frequency multiplexing, e.g., using several sources or a frequency-multiplexed SPDC source [20]. We refer to each such parallel attempt as a *multiplexing frame*.

Well-known LLEG protocols that fit this abstraction¹ include, for example, the three schemes based on SPDC sources described in [22], the Barret-Kok protocol [19] using emitters, and the single click scheme as described in [17]. Some of these protocols are further discussed in later sections, as we can further specialize our switch models based on the specific LLEG protocol used. Finally, we note that not all these LLEG protocols are suitable for all switch models described in the following sections. For example, some protocols (e.g., the midpoint source protocol with block-based attempts from [22]) may require memories at the switch, which is not compatible with the all-photon switch model in Section III.

III. LOGICAL MODEL 1: ALL-PHOTONIC SWITCH

This model of an *entanglement generation switch (EGS)* captures an all-photon switch with no quantum memories, N client nodes, multiple entanglement sources and an in-switch pool of B BSAs, that can be *re-bound* to port pairs. The BSMs are probabilistic and their outcomes are heralded back to the endpoints, but the switch does not perform any link-level heralding before attempting the BSMs. The scheduler's core decision is *which port pair each BSA listens to* so that incoming photons are routed to the same BSA. Since client nodes may have multiple sources (thus, a multiplexing degree S_i), several BSAs can simultaneously serve the same clients. Similar switching models appear in [7], [23], [9], [10].

A. System Formulation

The LLEG protocol between the switch and client i relies on S_i independent optical paths (e.g., fiber optic modes) into the switch's ingress ports. Time is slotted with duration Δt . Hardware calibration enforces a grouping of slots into epochs of T_{freeze} slots each. Each such interval is called a *freeze epoch*, during which the control decision is fixed and updated only between epochs [9]. We assume a constant T_{freeze} and negligible calibration time at epoch boundaries; if this overhead is non-negligible, all per-second rates derived later should be scaled by the corresponding active-duty factor (i.e., by the fraction of time spent in freeze epochs).

We set the slot duration to the LLEG attempt period and make two distinct modeling assumptions about heralding. First, the switch does not wait for *link-level* heralding before attempting BSMs: BSAs are committed to node pairs within an epoch and attempt BSMs blindly on the incoming photons. Second, at the *end-to-end* level, we assume that user nodes have sufficiently many local memories to buffer all tentative

Bell-pair halves across multiple slots until the classical BSM outcomes are heralded, focusing only on the resource constraints of the switch. Under this assumption, the start of the next slot is not delayed by end-to-end heralding, and the slot duration is not constrained by classical communication times.²

Control decisions: We assume that the BSAs in the switch, the per-node sources, and the physical links are homogeneous. Therefore, the scheduler's decision within a freeze epoch e is fully captured by the *station-allocation* variables $x_{ij} \in \mathbb{Z}_{\geq 0}$ (i, j) $\in \mathcal{F}$, denoting how many BSAs are reserved to serve client pair $(i, j) \in \mathcal{F}$ during epoch e . Feasibility is:

$$\sum_{(i,j) \in \mathcal{F}} x_{ij} \leq B, \quad \sum_{j < i} x_{ji} + \sum_{j > i} x_{ij} \leq S_i \quad (\forall i). \quad (1)$$

i.e., a global BSA budget and per-node source budgets. Let us denote the convex set defined by inequalities (1) as \mathcal{X} .

Per-link LLEG success: Per Sec. II-C, multiple LLEG protocols are possible. To illustrate the computation of $p_i(\beta)$, we consider a midpoint-source architecture (between node and switch) with a single photon-pair attempt per slot. Let $p_{\text{pair}}(\beta)$ denote the probability that the source successfully produces two entangled photons. We expect that, $p_{\text{pair}}(\cdot)$ is a strictly increasing function with respect to β (see Sec. II-C).

An LLEG attempt succeeds iff the photon latches onto the node memory and the partner photon reaches the BSA b within the BSM acceptance. The probability of a successful LLEG attempt is thus $p_i(\beta) = p_{\text{pair}}(\beta) (\eta_m g_m) (\eta_{\text{sw}} g_{\text{sw}})$. Here η_m captures half-link and coupling losses to the node memory, g_m the memory write/gate efficiency; η_{sw} captures half-link and routing to any station b , g_{sw} the temporal/spectral/mode acceptance at the BSM input.

End-to-end entanglement generation success: With exactly one LLE on each side of b , a coincidence attempt occurs in a slot iff *both* sources succeed and the photons are captured. Thus, for a BSA b serving (i, j) in epoch e ,

$$p_{ij}^{e2e}(\beta) = (p_i(\beta) p_j(\beta)) \xi^2 p_{\text{BSA}}. \quad (2)$$

Here ξ is the detector efficiency of every station b and p_{BSA} is the success probability of the optical Bell state analyzers. Below we sum up the operation of this type of switch:

Time-slot operation: (i) *Epoch allocation:* At the start of an epoch, choose $x_{ij}(e)$ satisfying inequalities (1) and configure any $x_{ij}(e)$ stations to serve (i, j) for the epoch. (ii) *Attempt:* Every node i performs up to S_i LLE attempts with identical success probability $p_i(\beta)$. (iii) *BSM:* BSMs are implemented with success probability (under homogeneity) $p^{e2e}(\beta) \triangleq p_{ij}^{e2e}(\beta)$ for every pair (i, j) . (iv) *Herald:* Upon success, the BSA sends the classical outcome to i, j . We assume that the next time slot begins immediately after the BSMs (step (iii)). That means that heralding occurs simultaneously and meanwhile each client node stores a Bell pair half in a

¹The discrete attempt abstraction is exact for pulsed sources [21]. For continuous wavelength sources [18], where pair inter-generation times are approximately Poisson with rate $\lambda(\beta)$, $p_i(\beta) = 1 - e^{-\lambda(\beta)\Delta t} \approx \lambda(\beta)\Delta t$ for $\lambda(\beta)\Delta t \ll 1$. We treat any success within a window as a Bernoulli trial registered at the slot boundary to fit in a discrete setting.

²If the BSA is slower than the source, or scarce node memories require waiting for end-to-end heralding before reuse, one can simply take the slot duration to be the dominant of these times. This only rescales the effective switching frequency and thus all per-second rates by a constant factor. Comparing the efficacy of the EGS architecture with and without the abundance-of-memories assumption for the nodes is left for future work.

dedicated quantum memory. For a graphical illustration of the EGS as well as its time-slot operation see Fig. 1(a) and 1(c) respectively.

B. Throughput Region

The expected number of end-to-end entanglement pairs for every pair i, j given x_{ij} is $p^{e2e}(\beta) x_{ij}$. We are interested in the *achievable* long term per slot service rates λ_{ij} for every pair i, j that can be achieved with these possible schedules. Collect these in a vector $\lambda = (\lambda_{ij})_{i < j}$ and define the *throughput region* Λ_{EGS} as the set of all such achievable vectors.

Recall that the convex set defined by inequalities (1) is denoted as \mathcal{X} . It is convenient to interpret \mathcal{X} in graph-theoretic terms. Consider the complete graph $G = (\mathcal{N}, \mathcal{F})$ with node set \mathcal{N} and edge set $\mathcal{F} = \{(i, j) : i < j\}$. For any integer vector $x = \{x_{ij}\}_{(i,j) \in \mathcal{F}} \in \mathbb{Z}_{\geq 0}^F$, the entry x_{ij} specifies how many units of capacity (or, equivalently, how many BSAs) are allocated to edge (or, equivalently pair) (i, j) . Constraints (1) then enforce that (i) the total number of such units does not exceed the budget B , and (ii) for each node i , the total number of units incident on i does not exceed S_i . In combinatorial-optimization terminology, any such $x \in \mathcal{X}$ is a capacitated b -matching of the complete graph with vertex capacities $b_i = S_i$ and an additional cardinality constraint of B units. The convex hull $\text{co}(\mathcal{X})$ can thus be viewed as a capacitated b -matching polytope augmented by this global budget constraint (e.g., [24]).

Let $\text{co}(\cdot)$ denote the convex hull of the set \mathcal{X} , then the set Λ_{EGS} is given by $\Lambda_{\text{EGS}} \equiv \text{co}(\mathcal{X}) \cdot p^{e2e}(\beta) / \Delta t$. Therefore, the throughput region is given by

$$\Lambda_{\text{EGS}} = \left\{ \frac{p^{e2e}(\beta)}{\Delta t} \cdot \lambda : \lambda = \sum_{x \in \mathcal{X}} \delta_x x, \right. \\ \left. \sum_{x \in \mathcal{X}} \delta_x = 1, \delta_x \geq 0, \text{ for all } x \in \mathcal{X} \right\}. \quad (3)$$

The set Λ_{EGS} contains all possible end-to-end entanglement generation rate vectors that an EGS can achieve. We dropped the dependency with β for ease of notation.

Maximum admissible total throughput: Λ_{EGS} is a high-dimensional polytope in \mathbb{R}^F induced by the feasible station allocations \mathcal{X} (constraints (1)). To quantify the “size” of Λ_{EGS} in terms of total throughput, we consider the maximum aggregate end-to-end rate per second:

$$R_{\text{EGS}}^{\text{sec}} \triangleq \max_{\lambda \in \Lambda_{\text{EGS}}} \sum_{(i,j) \in \mathcal{F}} \lambda_{ij} = \max_{\lambda \in \text{co}(\mathcal{X})} \frac{p^{e2e}(\beta)}{\Delta t} \sum_{(i,j) \in \mathcal{F}} \lambda_{ij}.$$

In other words, $R_{\text{EGS}}^{\text{sec}}$ represents the maximum L1 norm vector in the throughput region. Clearly, the limitation of this metric is that it does not give a holistic picture of the region. The main theorem of the section follows and provides a closed form formula for $R_{\text{EGS}}^{\text{sec}}$.

Theorem 1 (Closed form for maximum total throughput). *For the EGS model with B BSAs and per-node multiplexing*

degrees $\{S_i\}$, the maximum expected aggregate end-to-end success rate is

$$R_{\text{EGS}}^{\text{sec}} = \frac{p^{e2e}(\beta)}{\Delta t} E_{\text{EGS}}^{\text{max}}, \quad \text{where}$$

$$E_{\text{EGS}}^{\text{max}} = \min \left\{ B, \left\lfloor \frac{1}{2} \sum_i S_i \right\rfloor, \sum_i S_i - S_{\text{max}} \right\}, \quad (4)$$

and $S_{\text{max}} \triangleq \max_i S_i$.

We now present a lemma that gives intuition in $E_{\text{EGS}}^{\text{max}}$ and is useful for the proof of Theorem 1 as well as for the rest of the analysis.

Lemma 1. *Let \mathcal{X} be the integral polytope with $x = \{x_{ij}\}_{(i,j) \in \mathcal{F}}$ obeying inequalities (1). Then the maximum cardinality of a feasible allocation is $E_{\text{EGS}}^{\text{max}}$ in (4):*

$$\max_{x \in \mathcal{X}} \sum_{(i,j) \in \mathcal{F}} x_{ij} = E_{\text{EGS}}^{\text{max}}.$$

Both proofs of Lemma 1 and Theorem 1 are in the Appendix (Sec. VII-A and VII-B).

C. End-to-End Entanglement Fidelity

In addition to the throughput analysis, we now derive a closed-form expression for the fidelity of the end-to-end entangled state shared between any pair i, j following Sec. II-C.

Recall that, given an LLEG protocol, $w_i(\beta)$ denotes the Werner parameter associated with a successful LLE of node i (LLEG and link-level heralding in the switch related noise). Therefore, following Sec. II-B, the Werner parameter of the end-to-end entanglement between nodes i, j is

$$w_{\text{EGS}}^{e2e}(\beta) \triangleq w_i(\beta) w_j(\beta) q_{\text{BSM}} e^{-2L/(v_f T)},$$

where L denotes the link length and v_f the speed of light in the link. The last term, $e^{-2L/(v_f T)}$, corresponds to the Werner parameter related to the memory decoherence of the two end nodes’ entangled qubits from the time the switch learns about whether the LLEGs were successful until the end-to-end entanglement is heralded. This expression assumes that the end-to-end pair is used by the clients only after the end-to-end entanglement is heralded. Alternative models are possible (e.g., prepare-and-measure with postselection), in which case the relevant timing/decoherence window would be modified.

For demonstration, we further specialize this expression by assuming an LLEG protocol with midpoint sources on each link, which generate pairs with initial Werner parameter $w_0(\beta)$ (a decreasing function of β). Recall that τ_{hrld} denotes the classical-notification latency associated with link-level heralding, i.e., the time it takes for the switch to learn whether the client-switch link attempt succeeded. In the EGS model the switch does not wait for this information before attempting a BSM; rather, BSMs are triggered blindly and the subsequently received link-level heralds are used to determine whether that BSM attempt was valid (both links succeeded) or wasted (at most one link succeeded). Since we place the source in the middle of the link, after a successful link attempt a classical bit is transmitted from the node to the switch

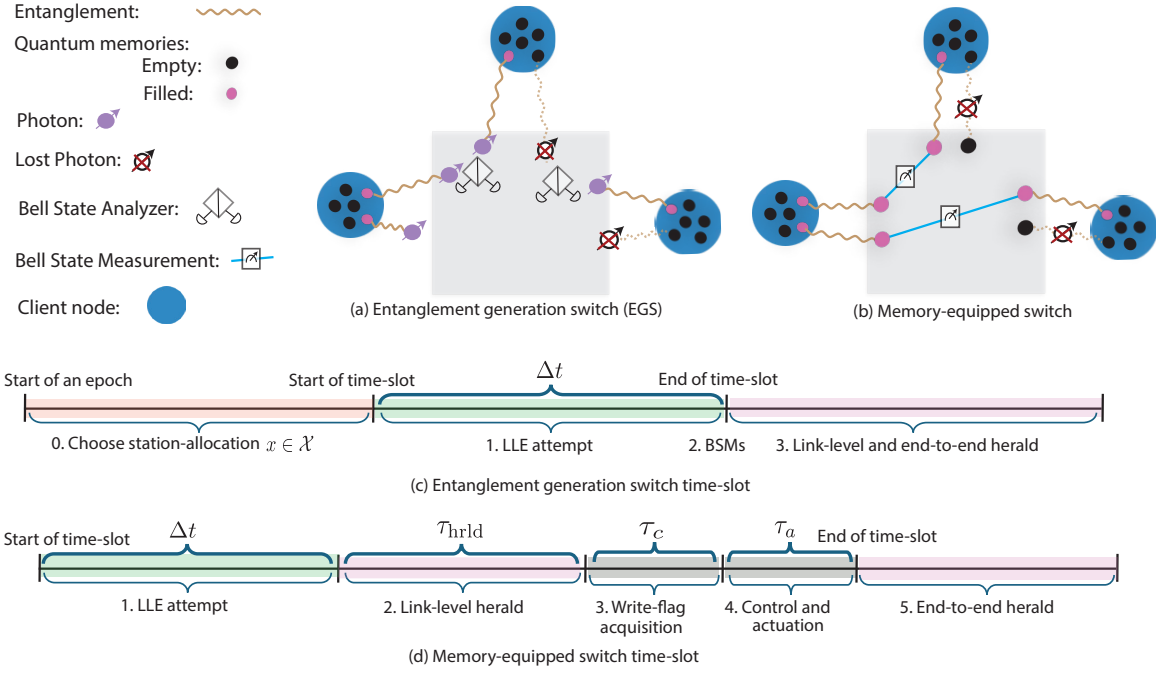


Fig. 1. Graphical illustration of (a) an EGS, (b) a memory-equipped switch, (c) the time-slot operation of an EGS, and, (d) the time slot operation of a memory-equipped switch. Both of the switches in illustrations (a) and (b) use $S_i = 2$ for every i , and $B = 2$. For the memory-equipped model in (b), $M_i = 2$ for every node i .

to report the link-level herald. Hence, $\tau_{\text{hrld}} = L/v_f$ and $w_i(\beta) = w_j(\beta) = w_0(\beta)e^{-\tau_{\text{hrld}}/T}$ for every pair i, j since, in this architecture, only the state in the nodes is stored in a memory while we herald the LLE (see Sec. III-A).

The corresponding end-to-end fidelity of the swapped pair is $F_{\text{EGS}}^{e2e}(\beta) = \frac{1+3w_{\text{EGS}}^{e2e}(\beta)}{4}$. Note that the end-to-end fidelity $F_{\text{EGS}}^{e2e}(\beta)$ scales with β as the square of $w_0(\beta)$.

IV. LOGICAL MODEL 2: QUANTUM SWITCH WITH INTERNAL MEMORIES (HERALD-THEN-SWAP CONTROL)

This section models and analyzes a near-term, memory-equipped switch and quantifies the benefit of *minimal* storage: storing photonic qubits in a memory only long enough for the switch to learn the slot's connectivity and make informed swap decisions. Similar models can be found in [11], [12], [15], [25]. This connectivity-aware control reduces wasted BSM attempts compared to the EGS and avoids the probabilistic optical-BSA bottleneck of EGS, but it increases decoherence due to additional storage time and lengthens the slot.

A. System Formulation

The switch can perform B BSMs per slot and has $M \geq 2B$ quantum memories that store single qubit states for one slot. The switch dedicates $M_i = S_i$ quantum memories to each client i (so that $\sum_i M_i = M$): each multiplexing frame of the LLEG protocol has a dedicated switch memory on its ingress channel.³ This simplifies the exposition and makes

³If $M_i \neq S_i$, only $\min\{M_i, S_i\}$ LLEs can be realized per slot; equivalently, in our analysis one can replace M_i by $\min\{M_i, S_i\}$ (the bottleneck).

this model a direct generalization of the EGS: each LLE can be *briefly* buffered at the switch until connectivity is known. Similar to the EGS architecture model, we assume that user nodes have sufficiently many memories to buffer all tentative Bell-pair halves until the classical BSM outcomes are heralded (i.e., during the end-to-end entanglement herald). Under this assumption, the next slot can start immediately after the BSMs.

Timing and slot-level operation. Let Δt_{mem} denote the duration of a time slot. For demonstration of this duration, we assume that each multiplexing frame corresponds to a mid-link source that attempts to emit one photon pair per pulse and each node memory tries to latch it. Δt_{mem} (and the associated qubit storage time) is determined by four serial latencies: (i) the duration of one LLEG attempt, Δt ,⁴ (ii) the classical overhead link-level heralding time, τ_{hrld} , (iii) write-flag+link-level heralds acquisition, τ_c , and, iv) control & actuation, τ_a :

$$\Delta t_{\text{mem}} = \Delta t + \tau_{\text{hrld}} + \tau_c + \tau_a.$$

In that case, $\tau_{\text{hrld}} = \frac{L}{v_f}$, where L denotes the node-switch fiber length and v_f the speed of light through the physical link. Moreover, $\Delta t = 1/f_{\text{pulse}}$. An explicit extension to block-based attempt LLEG protocols is developed in Sec. V-A.

$\tau_a > 0$ means that the switch needs time after it learns the connectivity to optimize the schedule. Hence, τ_a depends on the complexity of the scheduling algorithm. In the EGS, we

⁴This Δt can be shorter than the duration of a full LLEG attempt because emissions can be *pipelined* across slots. In particular, during the portion of a slot when the switch is busy with classical-processing/decision overhead, sources need not be idle: they may emit up to one one-way propagation time earlier so that the corresponding photons arrive at the start of the next slot.

implicitly assumed that τ_a is negligible since we stick to a control decision for $T_{\text{freeze}}\Delta t$ and do not need to change it in every time slot. While this is in principle possible in this model, it would require precomputing a distinct control action for every connectivity pattern, which is not scalable since the number of configurations grows exponentially in the number of clients. Operation within a slot t proceeds as follows

(i) *LLEG Attempt*: Every LLEG protocol carries out up to S_i attempts (ii) *Connectivity acquisition*: The switch receives heralding messages and stores the learned connectivity in an internal data structure. (iii) *Matching*: The controller computes and implements a memory-to-BSM mapping. (iv) *BSM*: Up to B selected memory pairs are measured out by the end of the slot. Recall that we assume infinitely many memories in the nodes so classical heralding of these BSM outcomes can take place afterward and can overlap with the next slot. If node memories are scarce, this delay of end-to-end entanglement herald can instead be absorbed into a larger effective slot duration. For a graphical illustration of the memory-equipped switch as well as its time-slot operation see Fig. 1(b) and 1(d) respectively.

LLEG success: The LLEG success probability under the midpoint link source, homogeneous memories assumption is $p_i(\beta) = p_{\text{pair}}(\beta)\eta_m^2 g_m^2$. This derivation is for the mid-link, single-attempt LLEG described above; the block-based attempt LLEG of [22] leads to a different expression, derived in Sec. V-A. Given $p_i(\beta)$, the connectivity $C_i(t)$ in slot t satisfies:

$$C_i(t) \sim \text{Binomial}(M_i, p_i(\beta)). \quad (5)$$

For each client i , the sequence $\{C_i(t)\}_t$ is i.i.d.

Control variables: After connectivity is learned, the switch observes $C(t) = \{C_i(t)\}_{i \in \mathcal{N}}$ and chooses a *matching of occupied memories across client indices*, i.e., $y_{ij}(t) \in \mathbb{Z}_{\geq 0}, (i, j) \in \mathcal{F}$, subject to the per-node supply and per-station budget, $\sum_{j < i} y_{ji}(t) + \sum_{j > i} y_{ij}(t) \leq C_i(t) \ (\forall i)$, and $\sum_{i < j} y_{ij}(t) \leq B$.

Swap success per attempt: Conditional on scheduling $y_{ij}(t)$ swaps for pair (i, j) , each attempt succeeds with p_{swap} . In the case of BSAs, $p_{\text{swap}} = \xi^2 p_{\text{BSA}}$. However, since in this model BSMs are carried out between memory qubits and not necessarily through linear optics, swaps can be deterministic (i.e., $p_{\text{swap}} = 1$) which is a benefit of memory-assisted switches. Hence, the number of end-to-end Bell states produced for the client pair (i, j) in slot t is $\mu_{ij}(t) \sim \text{Binomial}(y_{ij}(t), p_{\text{swap}})$.

B. Throughput Region

Let \mathcal{N} be the node set and $\mathcal{F} \triangleq \{(i, j) : i < j, i, j \in \mathcal{N}\}$. The *connectivity state space* is $\mathcal{C} \triangleq \prod_{i \in \mathcal{N}} \{0, 1, \dots, M_i\}$. A vector $c \in \mathcal{C}$ is a connectivity state. The random variable $C = C(t) = \{C_i(t)\}_{i \in \mathcal{N}}$ samples a connectivity state following (5). Since for every client i the sequence $\{C_i(t)\}_t$ is i.i.d., we can omit t when the time slot is not relevant. The probability mass function factorizes as

$$\pi(c) \triangleq \mathbb{P}\{C = c\} = \prod_{i \in \mathcal{N}} \binom{M_i}{c_i} p_i(\beta)^{c_i} (1 - p_i(\beta))^{M_i - c_i}.$$

Given a state c , the switch learns the available *supply* c_i of memories that have successfully established LLEs with node i and may schedule up to B BSMs. Let

$$\mathcal{Y}(c) \triangleq \left\{ y \in \mathbb{Z}_{\geq 0}^{\mathcal{F}} : \sum_{j < i} y_{ji} + \sum_{j > i} y_{ij} \leq c_i, \forall i, \sum_{(i, j) \in \mathcal{F}} y_{ij} \leq B \right\}$$

be the set of capacitated b-matchings in state c , with a global budget constraint of B units (see Sec. III-B). A vector $y \in \mathcal{Y}(c)$ is a valid schedule of BSMs given connectivity c . Its convex hull, $\text{co}\mathcal{Y}(c) \subset \mathbb{R}_{\geq 0}^{\mathcal{F}}$, captures all randomized time-sharing schedules conditioned on c .

A (possibly randomized) stationary, causal scheduling rule is a map $v : \mathcal{C} \rightarrow \text{co}\mathcal{Y}(c)$ that, for each observed state c , selects a convex combination of feasible matchings; equivalently, $v(c)$ is the expected pairing vector in that slot under some randomization over $\mathcal{Y}(c)$.

We are interested in the set of all achievable long-term end-to-end entanglement rate vectors λ , which we collect in the throughput region Λ_{mem} (in end-to-end pairs per second):

$$\Lambda_{\text{mem}} = \left\{ \lambda \in \mathbb{R}_{\geq 0}^{\mathcal{F}} : \exists v : \mathcal{C} \rightarrow \text{co}\mathcal{Y}(\cdot) \right. \quad (6) \\ \left. \text{s.t. } \lambda = \frac{p_{\text{swap}}}{\Delta t_{\text{mem}}} \sum_{c \in \mathcal{C}} \pi(c) v(c) \right\}.$$

Maximum admissible total throughput: Let $E_{\text{mem}}^{\text{max}}(c)$ denote the maximum number of swaps in state c , i.e.,

$$E_{\text{mem}}^{\text{max}}(c) \triangleq \max_{y \in \mathcal{Y}(c)} \sum_{(i, j) \in \mathcal{F}} y_{ij}.$$

To find a closed form for $E_{\text{mem}}^{\text{max}}(c)$, we use Lemma 1 by replacing S_i with c_i for every node i ,

$$E_{\text{mem}}^{\text{max}}(c) = \min \left\{ B, \left\lfloor \frac{1}{2} \sum_i c_i \right\rfloor, \sum_i c_i - \max_i c_i \right\}.$$

The maximum *expected* total end-to-end rate is then

$$R_{\text{mem}}^{\text{sec}} \triangleq \max_{\lambda \in \Lambda_{\text{mem}}} \sum_{(i, j) \in \mathcal{F}} \lambda_{ij} \\ = \frac{p_{\text{swap}}}{\Delta t_{\text{mem}}} \max_{v(\cdot)} \sum_{c \in \mathcal{C}} \pi(c) \sum_{(i, j) \in \mathcal{F}} v_{ij}(c) \\ \text{s.t. } v(c) \in \text{co}\mathcal{Y}(c) \quad \forall c \in \mathcal{C}.$$

Because the maximization decouples over c , this is

$$R_{\text{mem}}^{\text{sec}} = \frac{p_{\text{swap}}}{\Delta t_{\text{mem}}} \sum_{c \in \mathcal{C}} \pi(c) \max_{y \in \text{co}\mathcal{Y}(c)} \sum_{(i, j) \in \mathcal{F}} y_{ij}.$$

Since the objective is linear, the maximum over $\text{co}\mathcal{Y}(c)$ is attained at an extreme point, so

$$\max_{y \in \text{co}\mathcal{Y}(c)} \sum_{(i, j) \in \mathcal{F}} y_{ij} = \max_{y \in \mathcal{Y}(c)} \sum_{(i, j) \in \mathcal{F}} y_{ij} \triangleq E_{\text{mem}}^{\text{max}}(c),$$

and therefore

$$R_{\text{mem}}^{\text{sec}} = \frac{p_{\text{swap}}}{\Delta t_{\text{mem}}} \sum_{c \in \mathcal{C}} \pi(c) E_{\text{mem}}^{\text{max}}(c).$$

Obtaining a closed-form expression for the maximum expected total rate in this architecture is significantly harder

than in EGS (cf. Theorem 1). Nevertheless, since $R_{\text{mem}}^{\text{sec}}$ is an expectation, we can estimate it through Monte Carlo by sampling connectivities c .

C. End-to-End Entanglement Fidelity

Recall that, given an LLEG protocol, $w_i(\beta)$ denotes the Werner parameter associated with a successful LLEG of node i (LLEG and link-level heralding in the switch related noise). Therefore, the Werner parameter of the end-to-end entanglement between nodes i, j is

$$w_{\text{mem}}^{e2e}(\beta) \triangleq w_i(\beta) w_j(\beta) q_{\text{BSM}} e^{-4(\tau_c + \tau_a)/T} e^{-2L/(v_f T)}.$$

The term $e^{-4(\tau_c + \tau_a)/T}$ corresponds to the Werner parameter related to the memory decoherence that all of the four qubits involved experience after the link-level herald but before the BSM, whereas $e^{-2L/(v_f T)}$ corresponds to the decoherence of the two end node qubits from the BSM until end-to-end entanglement is heralded. Hence, $F_{e2e}^{\text{mem}}(\beta) = \frac{1+3w_{\text{mem}}^{e2e}(\beta)}{4}$.

For demonstration, we again assume a mid-link source that attempts one photon-pair per optical pulse, with each node memory trying to latch the first arriving photon. Recall that τ_{hrld} denotes the overhead time needed after the successful LLEG has been established to herald it in the switch. Since we place the source in the middle of the link, after an established LLE we need to transmit a classical bit from the node to the switch for the link-level herald in the switch. Hence, $\tau_{\text{hrld}} = L/v_f$ and $w_i(\beta) = w_j(\beta) = w_0(\beta)e^{-2\tau_{\text{hrld}}/T}$ for every pair i, j since now we have memories in both the node and the switch.

V. NUMERICAL RESULTS

We consider a default scenario reflecting near-term hardware parameters. Whenever we deviate from this set of parameters, we will state the changed parameter explicitly.

Baseline scenario: We consider $N = 6$ client nodes with multiplexing degree $S_i = 3$ and allow up to $B = 8$ concurrent BSM operations per slot. For BSAs in the EGS model, detectors have efficiency $\xi = 0.90$ and $p_{\text{BSA}} = 0.50$. For the memory assisted model we take $p_{\text{swap}} = 1$. The fiber attenuation is $\alpha = 0.2$ dB/km over a node-switch distance $L_{\text{node} \rightarrow \text{sw}} = 1$ km, so each half-link (0.5 km) has transmittance $\eta_{\text{fiber}, 1/2} = 10^{-\alpha(0.5)/10} = 0.98$ with $g_{\text{sw}} = g_m = 0.85$. For the LLEG protocol we use mid-link SPDC sources: we use the SPDC example of [26], where the probability of generating an n -pair coincidence is $p(n) = (n+1) \frac{\beta^n}{(\beta+1)^{n+2}}$. Under this model, the probability that the source emits photons is $\Pr(n \geq 1) = \frac{\beta(\beta+2)}{(\beta+1)^2}$ and the resulting initial fidelity is $F_0(\beta) = \frac{3w_0(\beta)+1}{4} = \frac{\Pr(n=1)}{\Pr(n \geq 1)} = \frac{2}{(\beta+1)(\beta+2)}$. We set $\beta = 0.03$ to get $F_0(\beta) = 0.96$. We assume $v_f = 2.0 \times 10^8$ m/s, yielding $\tau_{\text{hrld}} = 5$ μs , with $\tau_c = 2$ μs , $\tau_a = 3$ μs , and source pulse rate $f_{\text{pulse}} = 10$ MHz. Using these SPDC sources, we assume that the LLEG protocol for the EGS architecture is the single attempt protocol described in Sec. III, and for the memory-equipped architecture we use the optimal block-based LLEG protocol described in detail in Sec V-A. For fidelity-related

knobs we use $T = 500$ μs and $q_{\text{BSM}} = 0.97$. We approximate the stochastic variables using Monte Carlo with 10^5 samples.

A. Block-based LLEG Protocol in Memory-Equipped Models

In this section, we study the trade-offs between end-to-end entanglement rate, end-to-end fidelity, and users' utility in the memory-based model. We use our framework to show how a hardware designer can optimize the block size K , in a block-based attempt LLEG protocol.

Block-based attempt LLEG protocol: When the photon source employed by the LLEG protocol supports a fast pulse rate $f_{\text{pulse}} \gg 1/\Delta t_{\text{mem}}$, it is convenient to include K consecutive LLEG attempts at the beginning of a slot, and to load only the first successful photon in the switch's quantum memory [22]. Which photon is loaded is reconciled at the end of the block through classical heralding, and has to match between the two sides to have a success. No structural change is needed to incorporate this to our model, only a (block-size-dependent) adjustment to the qubit storage times, and an increased probability $p_i(\beta)$ for successful LLEG attempts.

Assuming amid-link source, the time-slot duration is

$$\Delta t_{\text{mem}} = (K-1)/f_{\text{pulse}} + \tau_{\text{herald}} + \tau_c + \tau_a. \quad (7)$$

Larger K increases latency but raises the LLEG success probability. Success occurs iff the first non-empty bin in the block delivers both photons. Let the per-bin outcomes be $q_2 = p_{\text{pair}}(\eta g_m)^2$, $q_1 = p_{\text{pair}}\eta g_m(1 - \eta g_m)$, $q_0 = 1 - p_{\text{pair}}(2\eta g_m - (\eta g_m)^2)$ (i.e., both, exactly one and none of the photons succeeding respectively). With K independent bins, the probability that the first non-empty outcome delivers both photons (i.e., the probability of a successful LLEG) is

$$\begin{aligned} p(\beta, K) &= \sum_{t=1}^K q_0^{t-1} q_2 = q_2 \frac{1 - q_0^K}{1 - q_0} \\ &= \frac{\eta g_m}{2 - \eta g_m} \left[1 - (1 - p_{\text{pair}}(\beta) \cdot (2\eta g_m - (\eta g_m)^2))^K \right]. \end{aligned}$$

The end-to-end entanglement fidelity also changes (from Sec. IV-C). Specifically, what changes with K is the time that the *successful* qubits spend in memories before the link-level herald in the switch and, consequently, the amount of decoherence. Let $T_{\text{succ}} \in \{1, \dots, K\}$ denote the index of the first bin in the block for which the outcome is "non-empty and good" (i.e., it yields the two photons that eventually define the link-level Bell pair). As in the success probability calculation above, the event that the first non-empty bin is t and delivers both photons has probability $\mathbb{P}\{T_{\text{succ}} = t, \text{ success}\} = q_0^{t-1} q_2$, $t = 1, \dots, K$, and the overall success probability is $p(\beta, K) = \sum_{t=1}^K q_0^{t-1} q_2$. Hence,

$$\mathbb{P}\{T_{\text{succ}} = t \mid \text{success}\} = \frac{q_0^{t-1} q_2}{p(\beta, K)}, \quad t = 1, \dots, K.$$

Under the midpoint-source assumption, a successful LLEG on link i corresponds to a mixture over possible success bins t , each inducing a different pre-link-level storage time. The Werner parameter associated with a successful LLEG on link i in the block-based protocol is therefore

$$w_i(\beta, K) = \frac{w_0(\beta)}{p(\beta, K)} \sum_{t=1}^K q_0^{t-1} q_2 \exp\left(-\frac{2}{T}(\tau_{\text{hrld}} + (K-t)\Delta t)\right).$$

Substituting this into the end-to-end expression (see Sec. IV-C), the Werner parameter of the shared pair between nodes i, j under the block-based LLEG protocol becomes $w_{\text{mem,block}}^{e2e}(\beta, K) \triangleq w_i(\beta, K) w_j(\beta, K) q_{\text{BSM}} e^{-4(\tau_c + \tau_a)/T} e^{-2L/(v_f T)}$.

Maximum aggregated throughput versus K and L : Fig. 2 contours how $\hat{R}_{\text{mem}}^{\text{sec}} \triangleq R_{\text{mem}}^{\text{sec}}/F$ varies with K and distance L . In panel (a), under the default values $\beta = 0.03$ and $f_{\text{pulse}} = 10$ MHz, a small L favors an optimal number of attempts of $K = 30$ (red dashed rectangles). As L increases, the link success probability drops, so a larger K is needed to maintain a high end-to-end rate; however, increasing K further becomes sub-optimal for the end-to-end rate because the slot duration grows per (7), reducing the attempt rate. As L continues to grow, the rate declines and changing K yields diminishing returns. In panel (b), increasing β to 0.15 brightens the map and shifts the optimum to lower K : higher single photon pair success lets us reduce K , which shortens the slot and improves rate. In panel (c), slowing the sources ($f_{\text{pulse}} = 1$ MHz) also lowers the optimal K , since each additional attempt increases the slot duration even more (see (7)).

Fidelity heatmap versus K and source rate: We examine the end-to-end fidelity as a function of K and f_{pulse} . The heatmap in Fig. 3 shows that for fast sources, fidelity is insensitive to K ; so K can be chosen to optimize solely the rate. In contrast, for slower sources, increasing K lowers fidelity. The reason is that each additional attempt lengthens the slot (cf. Eq. (7)), increasing memory storage time and thus decoherence. In general, raising K does not improve fidelity so the design problem is a rate–fidelity trade-off: increase K only if the rate gain justifies the fidelity loss.

End-to-end rate/fidelity trade-off via utilities: To study the joint trade-off between end-to-end entanglement rate R and fidelity F , we use proportional-fair utilities of the form $U = \log(RQ(F))$, following [17]. We consider three application-motivated choices for $Q(F)$ and thus U : (i) *distillable entanglement*, U_{DE} , with $Q(F) = D_H(F)$, the hashing yield (asymptotic one-way distillable entanglement); (ii) *secret-key utility*, U_{SKF} , with $Q(F) = S_{\text{BB84}}(F)$, the BB84 secret-key fraction; and (iii) *negativity utility*, U_{NGT} , with $Q(F) = \max\{F - \frac{1}{2}, 0\}$, a scaled entanglement negativity above the separability threshold. These utilities provide a single objective that balances throughput with quality and allow a comparison of hardware/model choices on equal footing. Since U_{DE} and U_{SKF} are only relevant for high fidelities ($F \gtrsim 0.85$), while the default scenario yields $F_{\text{mem}}^{e2e} \in [0.3, 0.8]$ (Fig. 3), below we use $L = 0.1$ km.

Fig. 4 plots $U_{\text{DE}}, U_{\text{SKF}}, U_{\text{NGT}}$ versus block size K . For comparable y-axis, we normalize the values of the utilities from 0 to 1. All three exhibit a unimodal, concave-like dependence, yielding a best block size K^* . K^* varies with the utility (i.e., target application) and the hardware parameters, enabling application-aware tuning of the parameters of the quantum switch. In the current setting, all three utilities preserve an optimal $K^* \in [4, 10]$.

B. Comparing EGS and Memory Switching

In this section, we compare the EGS and the quantum memory-equipped switch. Our goal is to identify which architecture *dominates* as the parameter regime changes and to provide guidance for hardware–model co-design. Although the results are specific to the chosen parameter regimes, our framework is general and can be applied to other parameters of interest for comparison. We use two complementary lenses: (i) the (R, F) *fidelity–rate frontier* obtained by sweeping the tuning parameter β , and (ii) an application-oriented *negativity utility* $U_{\text{NGT}} = \log(R \max\{F - \frac{1}{2}, 0\})$, which compresses each operating point into a single score aligned with entanglement usefulness. Whenever the memory model is used, we choose the optimal block size K^* for each setting— $K^*(\beta) \in \arg \max_K U_{\text{NGT}}(K, \beta)$. Thus K^* is case dependent.

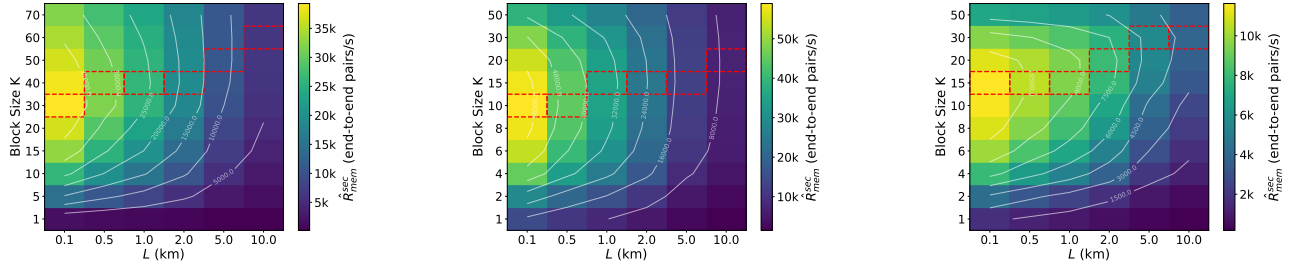
1) *Fidelity–Rate Frontier and Negativity vs. β* : We sweep the parameter $\beta \in [0, 0.15]$ and we compute the achievable normalized end-to-end rate $\hat{R}_{\text{mem}}^{\text{sec}}$ and fidelity F^{e2e} for the EGS and quantum memory-equipped switches.

In Fig. 5(a) observe that the curves trace the set of (R, F) versus β . Across large β , EGS achieves *both* higher rate and higher fidelity. However, in an intermediate high-fidelity window ($0.73 \lesssim F \lesssim 0.9$), the memory model becomes preferable: for the same target fidelity it delivers a higher rate. For very high fidelities ($F \gtrsim 0.9$) the memory model cannot reach the EGS curve because decoherence in the switch memories caps its attainable fidelity under this parameter set. In practice, an application can place a horizontal line at its required fidelity and read the *achievable rate* from Fig. 5(a). In Fig. 5(b), the negativity utility shows that for large β (corresponding to lower fidelities in Fig. 5(a)) EGS yields higher U_{NGT} , whereas for smaller β the memory model, with block size optimized for utility, attains higher U_{NGT} in the high-fidelity regime. Together, the two plots indicate that *model preference is regime-dependent*.

2) *Regime Sensitivity*: We vary key parameters to see how the ordering between EGS and the quantum memory-equipped switch changes. To keep a single, comparable score per operating point, we plot the *difference in negativity utility* $\Delta U_{\text{NGT}} \triangleq U_{\text{NGT}}^{\text{mem}} - U_{\text{NGT}}^{\text{EGS}}$ across β , and we indicate for each case, the fidelity interval over which the memory-equipped architecture dominates, inferred from the corresponding (R, F) plot as in Fig. 5(a). The (R, F) plots are omitted for space.

Source rate (Fig. 6(a)). Relative to the baseline, *slower* sources shift ΔU_{NGT} upward. The memory-equipped switch *dominates* because the slot is no longer a bottleneck and connectivity learning boosts rate while keeping fidelity high; for $f_{\text{pulse}} = 10$ kHz this corresponds to dominance over $0.65 \lesssim F \lesssim 0.92$. With *fast* sources (e.g., 1 GHz), $\Delta U_{\text{NGT}} < 0$ across all β (EGS *dominates*); the memory model wastes many entangled pairs awaiting for the heralding. However, this dominance assumes that nodes can store all states while awaiting heralding, which may be impractical at high f_{pulse} .

Length (Fig. 6(b)). Increasing L favors the memory-equipped switch and the β -interval where it dominates widens. Shorter heralding paths reduce decoherence and effective slot



(a) $\beta = 0.03$ and $f_{\text{pulse}} = 10$ MHz. (b) $\beta = 0.15$ and $f_{\text{pulse}} = 10$ MHz. (c) $\beta = 0.03$ and $f_{\text{pulse}} = 1$ MHz.
Fig. 2. Maximum total throughput $\hat{R}_{\text{mem}}^{\text{sec}}$ as a function of block size K and link length L ; red dashed rectangles mark the optimal K for each L .

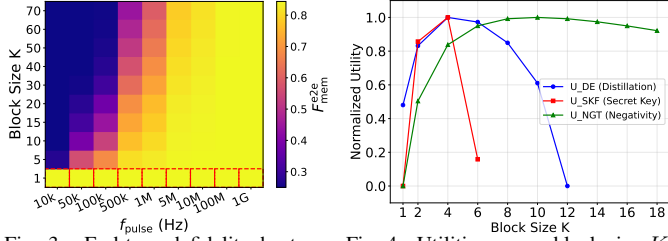
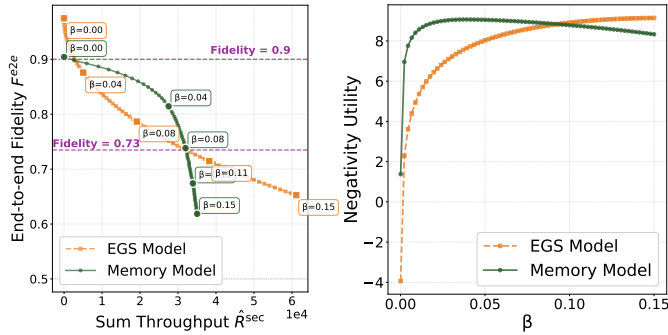


Fig. 3. End-to-end fidelity heatmap versus block size K and f_{pulse} . Fig. 4. Utilities versus block size K .



(a) Fidelity–rate frontiers w.r.t. β . (b) Negativity utility vs. β .
Fig. 5. Baseline comparison of EGS and memory-equipped switching.

duration, improving rate and fidelity for the memory design; in $L = \{0.1, 0.01\} \text{ km}$ it outperforms EGS for $0.66 \lesssim F \lesssim 0.93$.

Switch size (Fig. 6(c)). For larger switches, the curves are largely consistent with the baseline, supporting robustness of the conclusions.

VI. CONCLUSION

This work provides a unified framework to characterize the rate-fidelity tradeoffs between all-photonic and memory-equipped quantum switches. We demonstrate that while internal memories enable efficient herald-then-swap control, their advantage is regime-dependent, governed by the interplay of coherence times, heralding delays, and source rates. Future work should expand this analysis beyond near-term switches to include high-stability memories capable of supporting entanglement distillation and error correction, as well as exploring alternative switch architectures and LLEG protocols.

VII. APPENDIX

A. Proof of Lemma 1

Proof. Write $E^* \triangleq \max_{x \in \mathcal{X}} \sum_{(i,j) \in \mathcal{F}} x_{ij}$ and $T \triangleq \sum_i S_i$. We prove the lemma in two steps, first we prove that the maximum cardinality of a feasible allocation is upper bounded by $E_{\text{EGS}}^{\text{max}}$, and finally that it can achieve that value.

(I) *Upper bounds:* Every feasible allocation uses one station per selected edge, hence $E^* \leq B$. Each edge consumes one unit of capacity at two endpoints, hence

$$2 \sum_{(i,j) \in \mathcal{F}} x_{ij} \leq \sum_i S_i = T \Rightarrow E^* \leq \left\lfloor \frac{T}{2} \right\rfloor. \quad (8)$$

Finally, at most S_{max} edges can use the node with capacity S_{max} , and the remaining $T - S_{\text{max}}$ units of capacity reside at the other nodes. Even if all of that remaining capacity is paired with this node, we cannot realize more than $T - S_{\text{max}}$ edges. Therefore $E^* \leq T - S_{\text{max}}$ and hence $E^* \leq E_{\text{EGS}}^{\text{max}}$.

(II) *Achievability:* We wish to construct an integer vector $x \in \mathcal{X}$ attaining $E_{\text{EGS}}^{\text{max}}$. For now let us ignore B as a first step to construct the vector until we reintroduce it later in the proof of achievability. Consider a graph, in which for every node i we create S_i vertices. A feasible allocation corresponds to pairing vertices that correspond to distinct nodes, into unordered pairs; each pair (i, j) contributes one to x_{ij} (multiple pairs between the same (i, j) are allowed) and consumes one unit of residual capacity at both i and j .

We show that, without the station budget constraint $\sum_{(i,j) \in \mathcal{F}} x_{ij} \leq B$, the maximum number of such pairs equals

$$\tilde{E} = \min \left\{ \left\lfloor \frac{T}{2} \right\rfloor, T - S_{\text{max}} \right\}. \quad (9)$$

Case 1: $T - S_{\text{max}} \leq \lfloor T/2 \rfloor$. Pick a node i^* attaining $S_{i^*} = S_{\text{max}}$. Pair every unit of capacity on the other nodes with i^* . This uses $T - S_{\text{max}}$ pairs and respects per-node capacities: i^* contributes $T - S_{\text{max}} \leq S_{\text{max}}$ pairs, each other node j contributes at most S_j , and no self-pairs occur. Thus $\tilde{E} \geq T - S_{\text{max}}$, and by the upper bounds, equality holds.

Case 2: $T - S_{\text{max}} > \lfloor T/2 \rfloor$. Equivalently, $S_{\text{max}} < \lceil T/2 \rceil$. We prove that $\lfloor T/2 \rfloor$ pairs are always achievable via the following greedy rule: *Every node i starts with residual (i.e., unassigned) capacity S_i . At each step, select two distinct nodes $u \neq v$ with maximum residual capacities (ties arbitrary), add one to x_{uv} , and decrement both residual capacities by 1. Stop when fewer than two nodes have positive residual capacity.*

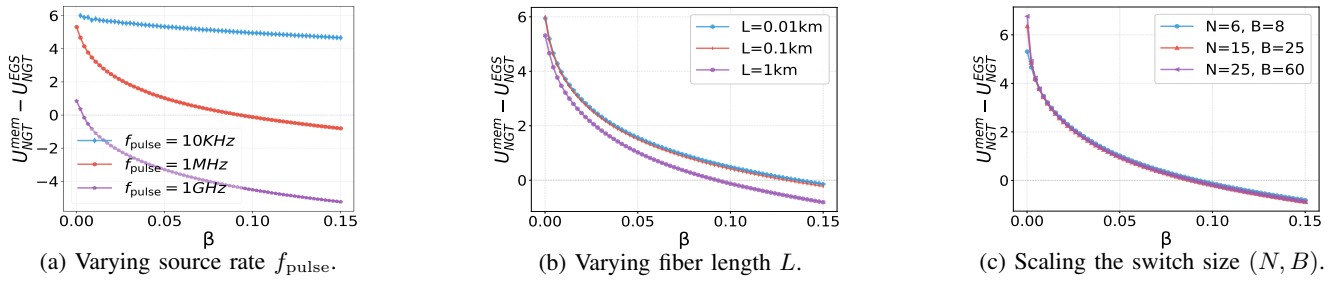


Fig. 6. Sensitivity of dominance using $\Delta U_{\text{NGT}}(\beta)$. Positive values favor the memory model; negative values favor EGS.

Let the residual capacities after k steps be $r_1^{(k)} \geq r_2^{(k)} \geq \dots \geq r_n^{(k)} \geq 0$, and let $T^{(k)} = \sum_i r_i^{(k)} = T - 2k$. Define the imbalance $\Delta^{(k)} \triangleq r_1^{(k)} - \sum_{i \geq 2} r_i^{(k)}$. Since $S_{\max} < \lceil T/2 \rceil$, $\Delta^{(0)} = S_{\max} - (T - S_{\max}) < T - 2\lceil T/2 \rceil < 0$. Each greedy step decreases $r_1^{(k)}$ and $\sum_{i \geq 2} r_i^{(k)}$ by exactly 1, hence $\Delta^{(k+1)} = \Delta^{(k)}$ for all k while the process runs.

Therefore $\Delta^{(k)} < 0$ throughout. If at some stage $T^{(k)} \geq 2$ but $r_2^{(k)} = 0$, then only one node is positive, so $\sum_{i \geq 2} r_i^{(k)} = 0$ and $r_1^{(k)} > 0$, implying $\Delta^{(k)} > 0$, a contradiction. Thus whenever $T^{(k)} \geq 2$ we must have $r_2^{(k)} \geq 1$, and the greedy step is always feasible. Consequently, the algorithm performs exactly $\lfloor T/2 \rfloor$ steps (until $T^{(k)} \in \{0, 1\}$). Each step produces one valid edge between distinct nodes, so we obtain $\lfloor T/2 \rfloor$ pairs. Therefore $\tilde{E} \geq \lfloor T/2 \rfloor$, and together with upper bound (8) we have $\tilde{E} = \lfloor T/2 \rfloor$. Therefore (9) holds.

What is left now to prove the achievability step of the proof is to reintroduce B , since in (9) we assumed no BSM budget constraints. Let $E_0 \triangleq \tilde{E}$ be the number of pairs constructed without BSM constraints. If $B \geq E_0$, we are done. If $B < E_0$, simply truncate the construction after B pairs. Truncation preserves feasibility. Hence, we have explicitly built $x \in \mathcal{X}$ with $\sum_{(i,j) \in \mathcal{F}} x_{ij} = \min\{B, \tilde{E}\} = E_{\text{EGS}}^{\max}$. Together with the upper bounds this proves $E^* = E_{\text{EGS}}^{\max}$. \square

B. Proof of Theorem 1

Proof. The objective $\sum_{(i,j) \in \mathcal{F}} \lambda_{ij}$ is linear over the polytope $\text{co}(\mathcal{X})$, so the maximum is attained at a vertex, which is an integral allocation $x^* \in \mathcal{X}$. Therefore,

$$R_{\text{EGS}}^{\text{sec}} = \frac{p_{e2e}(\beta)}{\Delta t} \max_{x \in \mathcal{X}} \sum_{(i,j) \in \mathcal{F}} x_{ij} = \frac{p_{e2e}(\beta)}{\Delta t} E_{\text{EGS}}^{\max},$$

where the last equality follows from Lemma 1. \square

REFERENCES

- [1] R. Van Meter, *Quantum networking*. John Wiley & Sons, 2014.
- [2] M. Caleffi *et al.*, "Distributed quantum computing: a survey," *Computer Networks*, vol. 254, p. 110672, 2024.
- [3] H.-J. Briegel, W. Dür, J. I. Cirac, and P. Zoller, "Quantum repeaters: the role of imperfect local operations in quantum communication," *Physical Review Letters*, vol. 81, no. 26, p. 5932, 1998.
- [4] G. Vardoyan *et al.*, "On the stochastic analysis of a quantum entanglement distribution switch," *IEEE Transactions on Quantum Engineering*, vol. 2, pp. 1–16, 2021.
- [5] S. Bhambay, T. Vasantam, and N. Walton, "Optimal scheduling in a quantum switch," *arXiv preprint arXiv:2501.05380*, 2025.
- [6] A. Einstein, B. Podolsky, and N. Rosen, "Can quantum-mechanical description of physical reality be considered complete?" *Physical review*, vol. 47, no. 10, p. 777, 1935.
- [7] S. Gauthier, G. Vardoyan, and S. Wehner, "An architecture for control of entanglement generation switches in quantum networks," *IEEE Transactions on Quantum Engineering*, vol. 4, pp. 1–17, 2023.
- [8] K. Azuma, K. Tamaki, and H.-K. Lo, "All-photonic quantum repeaters," *Nature communications*, vol. 6, no. 1, p. 6787, 2015.
- [9] S. Gauthier, T. Vasantam, and G. Vardoyan, "An on-demand resource allocation algorithm for a quantum network hub and its performance analysis," in *2024 IEEE QCE*, vol. 1. IEEE, 2024, pp. 1748–1759.
- [10] G. X. Yau, T. Vasantam, and G. Vardoyan, "Service-the-longest-queue among d choices policy for quantum entanglement switching," in *2025 International Conference on Quantum Communications, Networking, and Computing (QCNC)*. IEEE, 2025, pp. 1–8.
- [11] T. Vasantam and D. Towsley, "A throughput optimal scheduling policy for a quantum switch," in *Quantum Computing, Communication, and Simulation II*, vol. 12015. SPIE, 2022, pp. 14–23.
- [12] I. Tillman *et al.*, "Calculating the capacity region of a quantum switch," in *2024 IEEE QCE*, vol. 1. IEEE, 2024, pp. 1868–1878.
- [13] W. Dai, A. Rinaldi, and D. Towsley, "Entanglement swapping in quantum switches: Protocol design and stability analysis," *arXiv preprint arXiv:2110.04116*, 2021.
- [14] P. Promponas *et al.*, "Maximizing entanglement rates via efficient memory management in flexible quantum switches," *IEEE Journal on Selected Areas in Communications*, vol. 42, no. 7, pp. 1749–1762, 2024.
- [15] V. Valls, P. Promponas, and L. Tassiulas, "On the capacity of the quantum switch with and without entanglement decoherence," *IEEE Communications Letters*, vol. 27, no. 9, pp. 2388–2392, 2023.
- [16] N. K. Panigrahy *et al.*, "On the capacity region of a quantum switch with entanglement purification," in *IEEE INFOCOM 2023*. IEEE, 2023, pp. 1–10.
- [17] G. Vardoyan and S. Wehner, "Quantum network utility maximization," in *2023 IEEE QCE*, vol. 1. IEEE, 2023, pp. 1238–1248.
- [18] M. Alshowkan *et al.*, "Reconfigurable quantum local area network over deployed fiber," *PRX Quantum*, vol. 2, no. 4, Oct. 2021.
- [19] S. D. Barrett and P. Kok, "Efficient high-fidelity quantum computation using matter qubits and linear optics," *Physical Review A*, vol. 71, no. 6.
- [20] K. C. Chen *et al.*, "Zero-added-loss entangled-photon multiplexing for ground- and space-based quantum networks," *Physical Review Applied*, vol. 19, no. 5, May 2023.
- [21] P. Kok and S. L. Braunstein, "Postselected versus nonpostselected quantum teleportation using parametric down-conversion," *Physical Review A*, vol. 61, no. 4, Mar. 2000.
- [22] C. Jones *et al.*, "Design and analysis of communication protocols for quantum repeater networks," *New Journal of Physics*, vol. 18, no. 8, p. 083015, 2016.
- [23] S. Gauthier, G. Vardoyan, and S. Wehner, "A control architecture for entanglement generation switches in quantum networks," in *Proceedings of the 1st Workshop on Quantum Networks and Distributed Quantum Computing*, 2023, pp. 38–44.
- [24] A. Schrijver *et al.*, *Combinatorial optimization: polyhedra and efficiency*. Springer, vol. 24, no. 2.
- [25] P. Promponas, V. Valls, and L. Tassiulas, "Full exploitation of limited memory in quantum entanglement switching," in *2023 IFIP Networking*. IEEE, 2023, pp. 1–9.
- [26] P. Dhara *et al.*, "Heralded multiplexed high-efficiency cascaded source of dual-rail entangled photon pairs using spontaneous parametric down-conversion," *Physical Review Applied*, vol. 17, no. 3, p. 034071, 2022.